Atmos. Chem. Phys. Discuss., 12, 28609–28660, 2012
www.atmos-chem-phys-discuss.net/12/28609/2012/
doi:10.5194/acpd-12-28609-2012

Atmospheric Chemistry and Physics Discussions

The fine-scale structure of the trade wind cumuli over Barbados – an introduction to the CARRIBA project

H. Siebert[1,2], J. Bethke[1], E. Bierwirth[3], T. Conrath[1], K. Dieckmann[1], F. Ditas[1], A. Ehrlich[3], D. Farrell[4], S. Hartmann[1], M. A. Izaguirre[5], J. Katzwinkel[1], L. Nuijens[2], G. Roberts[6,7], M. Schäfer[3], R. A. Shaw[8], T. Schmeissner[1], I. Serikov[2], B. Stevens[2], F. Stratmann[1], B. Wehner[1], M. Wendisch[3], F. Werner[3], and H. Wex[1]

[1]Leibniz Institute for Tropospheric Research, Leipzig, Germany
[2]Max-Planck-Institute for Meteorology, Hamburg, Germany
[3]Leipzig Institute for Meteorology, University of Leipzig, Leipzig, Germany
[4]Caribbean Institute for Meteorology and Hydrology, Barbados, West Indies
[5]University of Miami, Miami, FL, USA
[6]Météo-France, Toulouse, France
[7]Scripps Institution of Oceanography, Center for Atmospheric Sciences, La Jolla, USA
[8]Michigan Technological University, Michigan, USA

Received: 28 September 2012 – Accepted: 25 October 2012 – Published: 31 October 2012

Correspondence to: H. Siebert (siebert@tropos.de)

Published by Copernicus Publications on behalf of the European Geosciences Union.

ACPD
12, 28609–28660, 2012

Abstract

The CARRIBA (Cloud, Aerosol, Radiation and tuRbulence in the trade wInd regime over BArbados) project with focus on trade wind cumuli over Barbados is introduced. The project is based on two one-month field campaigns in November 2010 (climatic wet season) and April 2011 (climatic dry season). Observations are based on helicopter-borne and ground-based measurements in a square of 100 km^2 off the coast of Barbados. CARRIBA is accompanied by long-term observations at the Barbados Cloud Observatory located at the East coast of Barbados since early in 2010 and which provides longer-term context for the CARRIBA measurements. Deployed instrumentation and sampling strategy are presented together with a classification of the meteorological conditions. The two campaigns were influenced by different air masses advected from the Caribbean area, the Atlantic Ocean, as well as the African continent which led to distinct aerosol conditions. Therefore, pristine conditions with low aerosol particle number concentrations of ~100 cm^3 were alternating with periods influenced by Saharan dust or aerosol from biomass burning resulting in comparable high number concentrations ~500 cm^3. The later was originating from both, the Caribbean area and Africa. The shallow cumulus clouds responded to the different aerosol conditions with a wide range of mean droplet sizes and number concentrations. Effective radii in the range of 7 to 18 µm have been observed. Finally, the four leading topics of CARRIBA – Clouds, Aerosol, Radiation and tuRbulence – are motivated and illustrated by selected findings and measurement examples.

1 Introduction and motivation

Shallow cumulus clouds are a common feature of the trade wind regions (hereafter called the trades). They play an important role in the moisture transport to the free atmosphere (Tiedtke, 1989) and for the Earth's radiation budget (Albrecht et al., 1995). Furthermore, shallow cumulus convection significantly influences the dynamics of the

ACPD
12, 28609–28660, 2012

sub-cloud layer (SCL) and cloud layer (CL) by intensifying the vertical transport of moisture, momentum, and heat from the surface to higher levels (Stevens, 2007).

Since the late 1940's the trades have been in the focus of the scientific cloud community. In a series of pioneering aircraft measurements known as the "Wyman and Woodcock Caribbean Expedition" in April 1946, soundings of wet and dry-bulb temperature in- and outside the clouds were performed. Based on these observations, new concepts of cloud dynamics and entrainment have been tested (Stommel, 1947, 1951). Malkus (1954, 1956, 1958) recognized trade wind cumuli as an example of convective processes under rather uniform and less complex conditions compared to cumuli forming over land in mid-latitudes.

Although the trades have been in the focus of several extensive field experiments since then, such as BOMEX (Barbados Oceanographic and Meteorological EXperiment) in 1968/1969 see Davidson (1968); Holland and Rasmusson (1973), ATEX (Atlantic Trade wind EXperiment) in 1969 see Augstein et al. (1973), or more recently RICO (Rain In Cumulus over the Ocean) see Rauber et al. (2007), or smaller campaigns such as BACEX (Barbados Aerosol Cloud EXperiment) in 2010, several aspects with regard to trade wind cumuli are still not understood in detail.

One of the most important open issues is the formation of precipitation. As the lifetime of trade wind cumuli is relatively short – in the range of hours – formation of precipitation through warm-rain processes is not expected. However, observations indicate the onset of precipitation sometimes in less than one hour. Already Langmuir (1948) pointed out that "... warm cumulus clouds often developed rain within less than thirty minutes after their formation...".

To clarify this warm-rain problem several topics need further investigation, such as the influence of small-scale turbulence on cloud droplet growth and the importance of atmospheric aerosol particles and cloud condensation nuclei (CCN) on the droplet number concentration, the droplet size, and the amount of drizzle forming from a cumulus cloud (e.g. Heymsfield and McFarquhar, 2001; Kaufman et al., 2005). Giant nuclei are supposed to play a particular role among the aerosol particles, as they might

ACPD
12, 28609–28660, 2012

promote the rapid development of precipitation, a topic which was mentioned and examined already by Woodcock et al. (1953) and which is still a topic of active research (e.g. Rudich et al., 2002; Blyth et al., 2003). In general, the role of the aerosol particles in controlling radiative properties of clouds may be important e.g. Twomey (1977), but the role of the aerosol in driving precipitation, particularly from shallow clouds, remains controversial (Stevens and Feingold, 2009). Quantitatively understanding of cloud controlling processes, particularly as relates to aerosol interactions with shallow cumulus, remains insufficient to advance the representation of these processes in numerical weather prediction and climate models.

Following Malkus' point of view, the trades provide unique laboratory conditions for investigating crucial cloud processes in conditions near stationarity. Furthermore, besides ship and aircraft emissions there are no significant anthropogenic aerosol sources upwind the island of Barbados, which we have chosen as basis for our observations, for several thousands of kilometers. Therefore, this place seems almost ideal to investigate the influence of aerosol layers advected by large-scale transport. In certain seasons, mineral dust advected from the Sahara is the dominant aerosol over Barbados (Prospero and Carlson, 1972; Smirnov et al., 2000; Reid et al., 2002). In addition, aerosol particles originating from biomass burning in Africa can frequently be observed from 1 to 4 km height (e.g. Haywood et al., 2008). The long-range transport of this aerosol type from the Sahara over the Atlantic and its influence on the Barbados region is discussed by Kaufman et al. (2005). Examining the influence of these aerosol particles reaching Barbados by large-scale advection or by production on the island itself, may shed light on the different aspects of shallow cumulus dynamics and the importance of aerosol particles therein.

Therefore, the CARRIBA-project (Cloud, Aerosol, Radiation and tuRbulence in the trade wInd regime over BArbados) was initiated by the Leibniz-Institute for Tropospheric Research (TROPOS) in Leipzig/Germany. The project is based on two one-month experiments with the ACTOS (Airborne Cloud Turbulence Observation System) and SMART-HELIOS (Spectral Modular Airborne Radiation measurement sys-

ACPD
12, 28609–28660, 2012

Tem) payloads along with ground-based aerosol characterization. The first campaign was performed in November 2010, at the end of the climatic wet season and is called $CARRIBA_{WET}$, the second campaign $CARRIBA_{DRY}$ was performed in the climatic dry season in April 2011. CARRIBA is embedded into a long-term initiative of the Max-Planck-Institute for Meteorology (MPI-M) in Hamburg/Germany, which operates the Barbados Cloud Observatory (BCO) located at the East coast of Barbados since early in 2010 and which provides longer-term context for the CARRIBA measurements.

With highly-sophisticated instrumentation such as the helicopter-borne ACTOS together with recently developed aerosol characterization methods, and collocated radiation observations with SMART-HELIOS in combination with ground-based spectral imaging sensors (see Sect. 2 for instrumentation), powerful tools were applied during CARRIBA to make a big step forward in understanding fundamental cloud and aerosol processes.

Beside the MPI-M the local Caribbean Institute for Meteorology and Hydrology (CIMH) on Barbados is a partner in this project and. In addition, long-term dust measurements which have continuously been performed since 1964 by the University of Miami are available from an upwind site at “Ragged Point”, a location at the eastern most tip of Barbados, where several systems for a thorough ground based aerosol characterization were additionally deployed for CARRIBA (see Sect. 4.2).

The main research interests of CARRIBA and the interplay of the related physical processes in and around a shallow cumulus cloud are illustrated in Fig. 1 together with a brief view of the sampling strategy with the two helicopter-borne measurement payloads. The objectives of CARRIBA in terms of four leading topics arise from the first four capitals of the campaign acronym and are briefly introduced below:

– Clouds: The cloud microphysical properties in terms of droplet number concentration and size distribution of trade wind clouds are investigated for different cloud regions and stages of cloud life time. Beside fundamental questions like how big droplets form in a turbulent shallow cumulus, the focus is on the question on how

ACPD
12, 28609–28660, 2012

the clouds do respond to different aerosol conditions observed during the two campaigns.

- Aerosol: The physical aerosol properties in the sub-cloud and cloud layer and the aerosol stratification are investigated for different meteorological conditions. One major topic in this context is how the aerosol particles control the cloud properties but also how clouds influence the aerosol conditions in the cloud layer.
- Radiation: The susceptibility of trade wind cumuli to different aerosol environments will be studied applying remote sensing techniques on the basis of measurements of spectral reflected solar radiation. The remote sensing results of optical and microphysical properties of trade wind cumuli will be compared with collocated in situ data.
- tuRbulence: The turbulent dynamics and thermodynamics of the sub-cloud layer, cloud environment, and cloud edges including the entrainment process are investigated. Furthermore, the turbulent in-cloud mixing and its influence on the cloud microphysical properties will be quantified by determining the governing time scales and dimensionless numbers.

This article is intended as a general introduction and overview of the CARRIBA-project for those interested in using the data, or considering similar measurement campaigns. After a classification of the weather situation observed during the two CARRIBA campaigns with emphasis on the cloud situation and the thermodynamic structure of the lower troposphere, measurement examples in the form of snapshots related to the four main themes of CARRIBA are presented. This compilation of different research topics is used to help motivate the project as a whole, and the sampling strategies that were employed.

ACPD
12, 28609–28660, 2012

2 Instrumentation and sampling strategy

2.1 Location of measurement sites and sampling strategy

The helicopter was operated from a helipad located at to the Concorde Experience Museum at Grantley Adams International Airport (GAIA, see map in Fig. 2). The main operational area was a roughly square area of 100 km^2 upwind of the BCO and Ragged Point sites which were supplemented with additional aerosol, meteorological and radiation measurements as part of CARRIBA (see map in Fig. 2). Typically, research flights began with a vertical profile up to a height of 2 to 3 km followed by several horizontal flight legs flown between two pre-defined navigation points (C1 and C2, see map in Fig. 2) separated by about 10 km and oriented in South-North direction. With this sampling strategy, the influence of the island was kept minimal and a direct comparison between helicopter-borne profiling, remote-sensing and radio-soundings at the BCO and aerosol measurements at Ragged Point is facilitated. During the second half of the flights, cloud sampling was performed in a semi-random fashion according to the present development and accessibility of shallow cumulus. To illustrate a typical flight pattern, one flight path of a two-hour flight (#18 from 10 April 2011, see Table 1 for an overview of all flight numbers and dates) is shown as a red line together with its corresponding height profile in the upper right part of Fig. 2. Blue lines indicate cloud penetrations. A second measurement area was defined in the south of the island as an alternative in case of possible conflict with commercial air traffic.

All flight paths from both campaigns have been included in Fig. 2 as thin lines (gray for CARRIBA$_{WET}$ and orange for CARRIBA$_{DRY}$). The three main operational areas are marked in Fig. 2 as colored boxes. About 80 % of cloud sampling was performed within the gray box (a), almost all profiling was performed within the green box (c) and four flights had to be performed in the orange box (b) due to conflicts with air-traffic. During CARRIBA$_{DRY}$, a few times low-level flight legs were flown about 50 m above sea level (a.s.l.) in order to investigate air-sea interaction. This has been done shortly after take-off while approaching point C1.

ACPD
12, 28609–28660, 2012

2.2 ACTOS and SMART-HELIOS

2.2.1 The ACTOS payload

During the two CARRIBA field campaigns, helicopter-borne measurements were performed with ACTOS (Siebert et al., 2006) which is an autonomous measurement payload carried by means of a 150 m long kevlar cable as external cargo. The long rope and a typical true airspeed of 20 m s^{-1} of the helicopter avoid any measurable influence of the rotor downwash. The overall length of ACTOS (Fig. 3) is about 5 m and the total weight is limited to 200 kg. The main body consists of five 19″ standard racks in which most of the sensor electronics, power supplies, and data acquisition systems are located. The sensors themselves are located on a carbon fibre outrigger on the front of ACTOS so as to avoid possible aerodynamic influences. A passive tail unit keeps ACTOS aligned in the mean flow direction.

ACTOS can be operated up to a height of about 3000 m and is restricted to shallow cumulus conditions, that is, deep convective clouds have to be avoided for safety reasons. Due to general flight rules, the helicopter remains above the clouds and ACTOS is dipped into the clouds from above. Due to the typical low gustiness observed in the trades, the wind speed was not a serious restriction for flight operation during the campaigns.

The standard ACTOS instrumentation comprises sensors for the wind vector, temperature, and humidity under clear and cloudy conditions. The measured wind vector is transformed into an Earth-fixed system using information about the payload position, attitude, and velocity taken from the GPS and inertial navigation systems (see Wendisch and Brenguier, 2013, for details). In addition to a PVM-100A (Gerber et al., 1994), which measures the integral properties of the cloud droplet spectrum, a Phase Doppler Interferometer (PDI) for single droplet measurements in the size range of 1 to 180 µm is included (Chuang et al., 2008; Wendisch and Brenguier, 2013).

ACTOS is additionally equipped with a variety of sensors to measure aerosol microphysical properties. The aerosol instruments are supplied by one common aerosol

ACPD
12, 28609–28660, 2012

inlet which is designed for sampling particles up to diameters of 3 µm. This ensures that cloud droplets cannot enter the system. The inlet is followed by a dryer to keep the relative humidity below 40 %. Aerosol particle number concentration (N_p) is detected by two CPCs (Condensation Particle Counters). The commercial TSI-CPC (model 3762, TSI Inc., St. Paul, USA; operated with a temperature difference between saturator and condenser of 25 K) measures N_p for particles larger than 6 nm with a measurement frequency of approximately 1 Hz. The second CPC measures particles larger than 8 nm with a frequency of 50 Hz (here-after referred to as Fast-CPC, see Wehner et al., 2011). The aerosol number size distribution was measured by a Scanning Mobility Particle Sizer (SMPS, see Wehner et al., 2010) providing a full spectrum between 6 and 230 nm at a time resolution of 2 min. For larger aerosol particles an Optical Particle Counter (OPC, model 1.129 "SKY-OPC", Grimm Aerosol Technik GmbH, Ainring, Germany) gives information about the aerosol number size distribution in the range of 300 to 2676 nm at a measurement frequency of 1 Hz. Additionally, a mini-CCNC (Cloud Condensation Number Counter) was used for measuring the CCN number concentration at different supersaturations (Roberts and Nenes, 2005). A similar instrument was also used in course of the ground-based aerosol characterization at the Ragged Point site during CARRIBA (see below). With the given true airspeed of ACTOS the spatial resolution for the Fast-CPC measurements are on the decimeter scale.

2.2.2 The SMART-HELIOS payload

The reflection of solar radiation by clouds was measured by SMART-HELIOS (see lower picture in Fig. 3). Two optical inlets for upward spectral radiance $I_\lambda^\uparrow$ and upward spectral irradiance $F_\lambda^\uparrow$ are connected with two plane grating spectrometers, for the visible (VIS, 300 to 1000 nm) and near-infrared (NIR, 900 to 2100 nm) spectral range. In the VIS the spectrometer has a full width at half maximum of 2 to 3 nm, in the NIR of 8 to 10 nm. $I_\lambda^\uparrow$ and $F_\lambda^\uparrow$ were sampled with a temporal resolution of 0.1 to 1 s. This temporal resolution and the opening angle of the radiance inlet of about 2° yield a spatial res-

ACPD
12, 28609–28660, 2012

olution of about 5 m, when SMART-HELIOS is measuring 140 m above the trade wind cumuli. Measurement uncertainties result from spectral and calibration uncertainties and are in the range of 6 % in the VIS and 10 % in the NIR. Observations of closely collocated in situ and cloud reflectivity data by ACTOS and SMART-HELIOS have been described in Henrich et al. (2010) and Werner et al. (2012).

SMART-HELIOS does not measure downward radiation due to its location close to the helicopter. This is a serious handicap because, as a consequence, the downward radiation has to be calculated. Therefore, additional ground based radiance measurements with the hyper-spectral imaging spectrometer AisaEAGLE were performed. The measurements were conducted at the BCO and were performed in parallel to all helicopter flights.

The AisaEAGLE is a single line sensor with 1024 spatial pixel that cover a field of view of 36.7° (Hanuš et al., 2008). By aligning the sensor perpendicular to the flow direction of the clouds, two-dimensional measurements of transmitted radiances (i.e. images of clouds) with high spatial resolution were obtained. For a cloud altitude of 2000 m the size of a single image pixel is about 1.3 m with 1300 m swath. The high resolution allows detailed studies of cloud edges. Schmidt et al. (2009) and Chiu et al. (2009) demonstrated that spectral radiation in the vicinity of clouds can be used to discriminate cloud and aerosol radiative effects.

For each spatial pixel AisaEAGLE measures the transmitted spectral radiance between 400 nm and 970 nm at 488 wavelength pixel. The spectral resolution is 1.25 nm full with at half maximum which is comparable to SMART-HELIOS and which allows to analyze the blueing effect of aerosol optical thickness in the presence of 3-dimensional cloud effects as proposed by Marshak et al. (2008).

2.3 Aerosol instrumentation at Ragged Point

During both CARRIBA campaigns, accompanying ground-based measurements were performed to obtain a continuous characterization of basic aerosol parameters for the duration of the campaigns. For this, we were able to use the facility operated by the

ACPD
12, 28609–28660, 2012

University of Miami at Ragged Point (see Fig. 2) where mineral dust measurements have been made continuously for more than forty years (Prospero and Lamb, 2003). An aerosol inlet on top of a 17 m high mast directly at the top of the cliffs at Ragged Point was used to sample the aerosol. Measurements were made in a ground based, air conditioned, container connected to the inlet by an inlet line. The aerosol was dried to a relative humidity below 25 % using diffusion dryers. The aerosol instrumentation operated at Ragged Point during CARRIBA included a DMPS (Differential Mobility Particle Sizer), with a DMA (Differential Mobility Analyzer, Type Vienna medium) and a CPC (model 3010, TSI Inc., St. Paul, USA) operating from 25 to 500 nm. Furthermore, a CCNC (Roberts and Nenes, 2005) measuring activation to cloud droplets for size segregated aerosol (i.e. operating in parallel to the DMPS-system); and a mini-CCNC (Roberts and Nenes, 2006), which measured total CCN concentrations, while the supersaturation was scanned from 0.1 % to 1 %, and is the counterpart to a sister instrument flown on ACTOS. The measured size distributions can be integrated to yield the total particle number concentrations N_p for the respective size range. Additionally to this instrumentation, daily filter samples were taken on top of the mast and analyzed with regard to the chemical bulk composition of the aerosol particles.

3 Classification of the two observational periods

In this section, an overview of the meteorological, cloud, and aerosol conditions during the two campaigns is provided. Cloudiness – in terms of cloud cover and the distribution of cloud base heights – and the humidity stratification during the two campaign periods will be compared with a two-year climatology. The latter is derived from two-year of RAMAN lidar and ceilometer measurements at the BCO, operational analysis from the European Center for Medium Range Weather Forecasts (ECMWF) and averaged ACTOS flight data. In Sect. 3.0.1 the different data sets are introduced which are then jointly discussed in Sect. 3.0.2.

ACPD
12, 28609–28660, 2012

3.0.1 The data

Figure 4 shows the volume depolarization ratio from the Raman lidar and the low-level (below 5 km) cloud cover derived from ceilometer data, both measured at BCO. The volume depolarization ratio can be considered a good dust indicator, but shows little sensitivity to aged aerosol particles produced by biomass burning. The upper panels show the time period from April 2010 to January 2012. The two CARRIBA campaigns are marked with colored boxes and enlarged in the lower panels. Rain showers are visible in the lidar data as short white gaps representing missing data, because the lidar system shuts down when rain is present. The long data gap at the beginning of $\text{CARRIBA}_{\text{WET}}$ is due to a power outage related to the hurricane Tomas that passed over Barbados.

Figure 5 shows profiles of specific humidity q, potential temperature θ and relative humidity rh derived from 12:00 UTC ECMWF operational analysis at a single grid-point near Barbados (300.66° E, 13.14° N), as well as the frequency of detecting cloud bases at any height derived from the ceilometer operating at the BCO. The dashed black lines in all panels indicate a two-year mean, from April 2010 to January 2012. Also shown are the mean profiles during days when ACTOS was flying, in solid black (OP ECMWF) and solid blue (ceilometer). The profiles measured by ACTOS during flight hours are shown in thick solid orange and red, similarly the cloud base heights measured during those flight hours by the ceilometer are shown in thick blue lines. We also show the mean RAMAN lidar humidity profiles between 07:00–09:00 UTC on ACTOS flight days. The RAMAN lidar only measures humidity profiles during nighttime (22:00–09:00 UTC), hence we choose the early morning 07:00–09:00 UTC timeframe to match the ACTOS flights closest in time. When comparing ACTOS with the OP ECMWF, one should keep in mind that the ACTOS flights were performed under favorable cloud conditions, implying that times with deep convective clouds and heavy rain showers were avoided, instead situations with typical trade wind clouds were preferred. This selection of flight times will bias the comparison in a certain way.

ACPD
12, 28609–28660, 2012

Mean values of selected quantities for each individual research flight have also been calculated after classifying the data into three categories: (i) data sampled in the SCL below 400 m. For this class only data sampled over the ocean are considered to minimize land effects. (ii) data in the height range between 700 m and 2 km but out off clouds, and (iii) all cloud data in the same height range. Here, cloud data is defined by a liquid water content (LWC) $> 0.05\,\mathrm{g\,m^{-3}}$. In this paper, we present the effective radius r_{eff} (see Fig. 6e) instead of the size distribution itself. The effective radius is calculated as the ratio between the third and second moment of the size distribution. The results are presented in Fig. 6 for both campaigns.

3.0.2 Discussion

The typical amount of precipitation in November is 170 mm (climatic wet season) compared with 60 mm in April (climatic dry season), based on a 30-yr record measured at the airport (period from 1981 to 2010). However, after a significant amount of precipitation at the end of October 2010 due to hurricane Tomas – on 30 October 2010 about 235 mm was measured, the highest daily value observed within the last 30 yr – November 2010 was comparable dry with only 65 mm. CARRIBA$_{\mathrm{DRY}}$ in April 2011 on the other hand experienced a total amount of precipitation of 143 mm, mainly due to a few days with heavy shower activity at the end of the month. Compared to the climatology, the CARRIBA$_{\mathrm{WET}}$ campaign was therefore much drier than the CARRIBA$_{\mathrm{DRY}}$ campaign, but because ACTOS flights took place mostly during non-raining periods, the unusual rain conditions did not bias the observations. In fact, in terms of the cloud field both campaigns experienced very similar conditions, with cloud cover frequently peaking above 0.5 (Fig. 4b) and the day-to-day variability being high (Fig. 4b, e, f).

During both campaigns the overall meteorology was quite similar, with easterly winds dominating and typical wind speeds being on the order of 5 to $10\,\mathrm{m\,s^{-1}}$ (Fig. 6a, b). During most flights, no significant vertical shear was observed, that is, the wind velocity was similar in the SCL and the CL. Only for a four-day period in November 2010 (20 to 24) the wind record indicates some vertical shear with stronger winds in the SCL

ACPD
12, 28609–28660, 2012

compared to higher levels. A second exceptional period took place in April 2011 when the trades were disturbed for a three-day period between 18 to 21 April and the wind in the SCL turned to north-east whereas winds in the CL were from the south-west. This period coincided with the weakest wind speed observed during the two campaigns, $U < 5\,\mathrm{m\,s^{-1}}$ (cf. Fig. 6b).

The prevailing easterlies in combination with a quite constant sea-surface temperature resulted in quite stable temperature conditions in the SCL (over water) with $\overline{\Theta} = 300.6\,\mathrm{K}$ in November 2010 compared with $\overline{\Theta} = 299.3\,\mathrm{K}$ in April 2011 (Fig. 6d). The day-to-day variation of the mean temperature in the SCL was typically below 0.5 K. The specific humidity (Fig. 6c) during both campaigns had a mean value around $17\,\mathrm{g\,kg^{-1}}$ and a standard deviation of $\sim 1\,\mathrm{g\,kg^{-1}}$, based on all flights. The two days with the lowest observed humidity values in the SCL (morning flight on 21 November 2010 and 9 April 2011) were the only two flights without any clouds in the measurement area. Both days show also the lowest temperatures in the SCL (Fig. 6d).

Evidently, the mean q-profiles measured with ACTOS, as well as with the RAMAN lidar, are 1 to $2\,\mathrm{g\,kg^{-1}}$ moister compared to the OP ECMWF profiles during both $\mathrm{CARRIBA_{WET}}$ and $\mathrm{CARRIBA_{DRY}}$, especially in the SCL during April 2011 (Fig. 5a). Radiosondes launched over the island, that are used in the data assimilation performed at ECMWF in producing their analysis, also show a drier lower atmosphere. Because the ACTOS profiles are derived from highly accurate fast dewpoint mirror measurements performed over the open ocean, and the RAMAN lidar is also located directly at the coastline, land-ocean differences, especially in the SCL, may play a role in explaining these differences.

Because the mean ACTOS profiles are based on only one profile per flight, per day, and the water vapor field is highly variable in both space and time, one should keep in mind that ACTOS profiles likely do not represent the mean conditions during these months. Based on the ECMWF OP and the RAMAN lidar profiles, we believe that ACTOS flights were performed under somewhat warmer and moister conditions during $\mathrm{CARRIBA_{WET}}$, and drier and colder conditions during $\mathrm{CARRIBA_{DRY}}$. These

ACPD
12, 28609–28660, 2012

combined lead to little difference in the relative humidity profiles in the SCL, and little differences in the overall frequency of detecting cloud, although cloud fraction near cloud base (500 m) was somewhat higher during $\text{CARRIBA}_{\text{WET}}$. Again, because the ACTOS means are based on just a few profiles, the high θ and low rh in the SCL during $\text{CARRIBA}_{\text{WET}}$ should not be taken as representative.

Both the ECMWF OP and ACTOS profiles show that the rh in the lower cloud layer, between 700 m and 1.8 km, was higher during $\text{CARRIBA}_{\text{DRY}}$, but at heights above 2 km, both q and rh decrease more sharply compared to $\text{CARRIBA}_{\text{WET}}$. This indicates a stronger inversion during $\text{CARRIBA}_{\text{DRY}}$. Indeed, during April months the large-scale subsidence (not shown) is generally stronger than during November months, leading to a more stable and drier atmosphere. The peak in detected cloud base heights just above 2 km $\text{CARRIBA}_{\text{DRY}}$ indeed reflects a more frequent occurrence of extended cloud layers near cloud top that likely result from this stronger inversion.

The aerosol particle number concentration N_{p} observed during ACTOS flights (Fig. 6f) is in general on the order of a few hundred particles cm^{-3} (Fig. 6b). Typically, the concentration in the SCL and in higher levels is quite similar and there is only a small decrease of N_{p} with height. Only the westerly winds on 18 to 21 April 2011 advected a significantly increased aerosol particle number concentration at higher levels.

At the beginning of $\text{CARRIBA}_{\text{WET}}$ (11 to 13 November) and from 17 to 19 November, Barbados was significantly influenced by advected Saharan dust which is visible in the volume depolarization ratio of the lidar in Fig. 4. The dust layers reached heights of up to 2 to 3 km but a significant amount of dust was also mixed down and increased particle number concentration was observed at Ragged Point (see concentration in Fig. 6 for particles > 80 nm). Unfortunately, for the second dust period no flight data is available. For both periods, air masses originated from regions in Africa with biomass burning were mixing with Saharan dust influenced the situation in Barbados. However, biomass burning aerosol does not contribute to the volume depolarization ratio but results in a generally increased particle number concentration. During a third period between 25 and 26 November an increased volume depolarization ratio in the lidar

ACPD
12, 28609–28660, 2012

signal was observed in a layer roughly between 1 and 2 km indicating again advected dust. During this period the downward mixed dust resulted in a slightly reduced lidar signal compared to the main layer. In-situ data at Ragged Point and from ACTOS do well agree with the lidar observations. The slightly higher concentrations observed by ACTOS result from particles smaller 80 nm. Again, aerosol originated from biomass burning was partly influencing the situation over Barbados. During clean periods, for example around 21 November, often increased number concentrations of Aitken-mode particles (< 80 nm) were observed which were attributed to freshly produced particles.

For CARRIBA$_{DRY}$, we can divide the campaign into three major periods in terms of aerosol load. The first half of CARRIBA$_{DRY}$ was influenced by Saharan dust layers in a height up to 3 km height indicated by an increased volume depolarization ratio. This period was interrupted by a comparable clean period (8 to 12 April) which coincides with higher cloudiness but no precipitation. Partly the dust was mixed down leading to increased number concentration at ground. The dust disappeared completely on 17 April when the wind in the SCL turned to more north-east direction advecting clean marine air masses. About 50 % of the aerosol particle concentration at ground was caused by Aitken-mode particles < 80 nm in the SCL for all the flights performed from 18 to 20 April. In the cloud layer the weak wind from south-west was advecting air masses from the Caribbean area (Fig. 6). Thus, this cloud layer was influenced by extensive biomass burning activity observed in the entire Caribbean area and also on Barbados (see MODIS fire maps for the period from 17 to 21 April, not shown here) resulting in particle number concentrations up to 800 cm^{-3} – the highest mean values observed during the two campaigns. Therefore, although the mean particle number concentrations in the SCL and CL are comparable, the reason for the high numbers is completely different. A period with low aerosol burden and the lowest observed CCN concentration of $\sim$ 60 cm^{-3} was observed from 22 to 24 April. Again, on 24 April 2011 there was a very high concentration of Aitken mode particles with a peak around 30 to 40 nm which results in an increased total number concentration but low CCN concentration.

ACPD
12, 28609–28660, 2012

The clouds usually respond to a changing aerosol number concentration in the SCL in a well known way, where with decreasing aerosol particle number concentration the droplets will become bigger. As a measure for the mean size of the cloud droplets, Fig. 6e shows the effective radius derived from the droplet size distributions together with the retrieved values from the radiation measurements. A detailed analysis of the droplet size distributions of different cloud types under different aerosol conditions will be published elsewhere. The range of in-situ observed r_{eff} is from 7 to 18 µm. The highest values of r_{eff} have been observed at the end of CARRIBA$_{DRY}$, identified as a period with the lowest aerosol number concentrations for particles > 80 nm in the cloud layer. The smallest cloud droplets in terms of r_{eff} have been measured in the period where the trades were disturbed and the aerosol laden air-masses from the Caribbean region where prevailing over Barbados.

In general, during phases when aerosol was advected from Africa during CARRIBA$_{WET}$, it was often a mixture of dust and biomass burning, both originating from the African continent. In contrast, for respective phases during CARRIBA$_{DRY}$, the aerosol could be characterized as dust events, resulting in higher volume depolarization ratios. A further difference between the two campaigns was, that during CARRIBA$_{DRY}$ we took measurements within air-masses originating from the Caribbean region with enhanced particle number concentrations due to biomass burning.

4 The four leading topics of CARRIBA

In this section the observations related to CARRIBA's motivating themes – clouds, aerosol, radiation, and turbulence – (cf. Fig. 1) are discussed by presenting selected findings and a general discussion of the observations.

ACPD
12, 28609–28660, 2012

4.1 Cloud properties

Cloud properties in terms of droplet diameter, droplet number concentration, and LWC have been investigated for different meteorological and aerosol conditions during both campaigns. Most of the flights have been performed in fields of typical trade wind cumuli with a horizontal extend of a few hundred meters and a vertical extend of about 1 km. Due to a nearly constant sea-surface temperature of 25 °C, the lifting condensation level was around 500 m, but often evaporating cloud remnants with higher cloud base were observed. Often, also thin stratiform cloud layers stretching across the upper part of the cumulus layer were observed, most probably due to detraining cumulus clouds in combination with locally stable stratification.

Figure 7a shows an example of cloud droplets measured by the PDI with two different types of clouds. The green box assigns measurements performed during the traverse of a stratiform cloud layer, the black box represents typical trade wind cumuli. Furthermore, there is evidence of abundant large particulate matter in the cloud free air (red box), which will be discussed later on.

The droplet size range of the stratiform cloud layer is about 1 to 50 µm and narrower than what is typically observed in the shallow cumulus clouds, which frequently include a long-tailed distribution indicative of an active coalescence process (see Fig. 7b).

As can be seen in Fig. 7a, there are substantial particle counts associated with large particles in the cloud free regions of the SCL and CL. Since the PDI is configured in a way that does not allow it to see non-spherical particles with refractive indices substantially different from that of water it is unlikely that these particles are associated with dust. Therefore, we conclude that the measured particles are dissolved sea salt particles with a size range of 1–20 µm, which experienced hygroscopic growth and are in thermodynamic equilibrium e.g. not activated. Their number concentrations are relatively small (0.5 to 1 cm^{-3}) compared to typical cloud droplet number concentrations of ~100 cm^{-3} (see also Fig. 7b).

ACPD
12, 28609–28660, 2012

Figure 8a depicts the vertical profile of the particle diameter, rh, and the Θ for the first ascent. A positive correlation with rh becomes obvious with particles being smaller at altitudes where rh is decreasing, and particles being larger where rh shows an increase. Apart from this hygroscopic behavior, the particles have a rather constant mean size of about 5–6 µm. The larger particle sizes and number concentrations at heights of about 2200 m are most likely due to the fact, that these measurements were performed close to clouds and thus, the challenge will be to sort out to what extent these are evaporating drops versus dissolved sea-salt particles. In Fig. 8b the vertical profile of the particle number concentration, as well as rh, is shown for the first ascent of this flight. A positive correlation between number concentration and rh becomes obvious. Due to the hygroscopic nature of sea salt, particles tend to decrease in size with decreasing rh until they become too small to still be detected by the PDI.

4.2 Aerosol processing in the sub-cloud and cloud layer

4.2.1 Ground-based versus airborne measurements

Figure 9a shows a selection of three different aerosol particle number size distributions (here-after simply called size distribution), which are averages from continuous ground measurements at Ragged Point (thick lines) done during three different research flights with ACTOS (flights #06, #13, and #14). Additionally, Fig. 9a shows simultaneously determined size distributions in the SCL in heights up to 400 m (thin lines). In general, the agreement between the measurements taken on ground and those taken on ACTOS inside the SCL is good, indicating that the ground based measurement might be used to describe the aerosol observed in the SCL.

A common feature of all the size distributions shown in Fig. 9a is a pronounced minimum in the particle number concentration at particle diameters of around 70 nm to 90 nm. This minimum is often referred to as the Hoppel-minimum after Hoppel et al. (1986), which indicates the size above which particles have been activated to a cloud droplet before, a process during which additional soluble mass due to wet phase chem-

ACPD
12, 28609–28660, 2012

istry is acquired (e.g. Yuskiewicz et al., 1999). The diameters at this minimum can be interpreted as being indicative of the average peak supersaturation found in the cloud. Assuming an average hygroscopicity for marine aerosol particles in the North Atlantic as given in Pringle et al. (2010) of about $\kappa = 0.59$ (with κ as defined in Petters and Kreidenweis, 2007), these maximum supersaturations can be derived to be on the order of 0.2 % to 0.3 %. Figure 9b shows a selection of size distributions recorded on ACTOS during flight #06 at cloud level. All black lines indicate size distributions which are recorded in the vicinity of clouds show a bimodal distribution with a well pronounced Hoppel minimum as measured on ground and in the SCL. Instead, the thick blue lines representing the interstitial aerosol feature a mono-modal distribution, where the accumulation mode (particles larger than e.g. $d_p = 100$ nm) vanishes due to cloud droplet activation.

4.2.2 Vertical distribution of total aerosol and CCN number concentrations

The three flights shown in Fig. 9 were chosen to describe three typical marine aerosol number size distributions. All shown size distributions feature a bimodal distribution. In contrast the number concentration of the individual modes varies which has a large effect on the CCN concentration. The size distributions during flight #06 show two modes with comparable low concentration, while the size distributions during flight #13 feature a dominating Aitken mode (particles between 20 nm and 80 nm in diameter) and the size distributions during #14 a dominating accumulation mode.

Figure 10 shows three vertical profiles of the measured aerosol particle number concentration (panel b) and CCN concentration (panel a) at a supersaturation of 0.26 % for the same periods during which the size distributions shown in Fig. 9 were measured. At this supersaturation the concentration of CCN is mainly dependent on the number concentration of aerosol particles larger than the Hoppel-minimum. During #06 and #13 CCN concentrations are similar, although there were many more small particles during #13, which is also obvious in the vertical profiles of N_p in Fig. 10b. In comparison, the increase in the number of particles in the accumulation mode during #14 is

ACPD
12, 28609–28660, 2012

well reflected in the doubling of the CCN concentration. In these examples CCN concentrations are fairly stable up to around 1200 m. Above this height the concentration shows a first decrease, with the drop most pronounced for #14, and drops further at about 2200 m near the transition to the free troposphere. The vertical profiles of N_p in Fig. 10b show a more variable pattern in heights above 1200 m. In contrast to the CCN concentration, the total aerosol concentration not necessarily drops when reaching the free troposphere, indicating a change in the shape of the size distributions and an increase in the concentration of small particles.

In the previous section, the relation between aerosol particles and clouds was mainly discussed in terms of particles acting as nuclei for cloud droplet condensation. However, clouds should also be considered as a source of aerosol. The conditions around clouds are supposed to be favorable for new particle formation, e.g. nucleation and subsequent particle growth. High actinic fluxes, increased humidity with comparable low temperatures in combination with reduced particle surface area seem to be favorable for new particle formation. Signs of new particle formation in combination with clouds in comparable clean environments have been observed by Perry and Hobbs (1994) who found freshly produced particles in the outflow of deep convective clouds in a height of around 4 to 5 km.

During both CARRIBA campaigns signs of new particle formation have been frequently observed. Almost all flights with clouds exhibit at least a few distinct events, e.g. particle number concentrations increased by about one order of magnitude compared with the background concentration. Only for days with general high aerosol load and higher particle surface area no signs of new particle formation have been observed (e.g. 19 April 2011 was a day with high particle number concentrations on which no new particle formation was observed).

Figure 11 shows a 6 km-long flight path in around 900 m height with a few cloud penetrations indicated by the LWC signal (black line in panel a). The red line in panel a indicates the total particle number concentration sampled at 100 Hz with the Fast-CPC in the size range of 6 nm to 2 µm. The few distinct spikes indicating new particle

ACPD
12, 28609–28660, 2012

formation are striking. Many of them can be directly related to clouds or more precisely to cloud edges. However, a few of them do not correspond to any significant changes in other parameters such as w (panel b) or T and a in panel c. The first new particle formation event in panel a is enlarged for a better insight. It is quite obvious that new particle formation is linked to the humid cloud environment but sometimes the areas with increased particle number concentration seems to grow into the cloud region. Since the horizontal extent of this process is limited to a few decameters or so, the slow flying ACTOS with the new Fast-CPC is highly suitable for such investigations.

4.3 Radiation properties of trade wind cumuli

Time series of trade wind cumuli optical and microphysical properties (cloud optical thickness τ, effective droplet radius r_{eff}) were derived from the time series of upward spectral radiances $I_{\lambda}^{\uparrow}$ and look-up tables calculated with the *libRadtran* 1.6b radiative transfer package (Mayer and Kylling, 2005; Mayer, 2009). τ and r_{eff} are used to derive $\text{LWC} = 2/3 \cdot \tau \cdot r_{\text{eff}} / (\rho \cdot z)$, with the density of liquid water ρ and the vertical extent of the trade wind cumuli z estimated from LIDAR and ACTOS measurements. Uncertainties in retrieved τ and r_{eff} arise from the measurement errors in $I_{\lambda}^{\uparrow}$ and uncertainties in the radiative transfer calculations. They are in the range of 3% and 9% for τ and r_{eff}, respectively.

The retrieved cloud properties were compared to the in situ measurements by the PVM-100A on ACTOS. The mean values of r_{eff} and LWC for each flight agree within 2 to 3 µm and about 0.06 g m^{-3}, respectively. Due to the high time resolution and close collocation of both instruments, time series of individual clouds can be analyzed. Figure 12 a shows a time series of τ, Fig. 12b) of r_{eff} and Fig. 12c of the LWC over a single trade wind cumulus on 22 April 2011.

In general, both data sets agree within their respective measurement uncertainties, although discrepancies attributable to different sampling strategies are evident.

ACPD
12, 28609–28660, 2012

Directly at the beginning of the time series and at around 1500 m, ACTOS measurements indicate a cloud gap, while the retrieval results yield cloud data with r_{eff} = 9 to 15 µm and LWC = 0.2 to 0.4 g m^{-3}. Such instances regularly occur when ACTOS briefly dips outside of cloud top, while the SMART-HELIOS payload still gathers data above the cloud. Larger differences in r_{eff} and LWC, as illustrated at around 1400 m, occur when both instruments probed different cloud areas (e.g. ACTOS measuring up to 100 m below cloud top) or when cloud inhomogeneities caused 3-D–radiative effects. Moreover, in the calculation of the retrieved LWC a constant cloud height is assumed for each measurement flight. Trade wind cumuli, even though only a couple of 100 m in vertical extent, show rather large inhomogeneities and the cloud top height might vary considerably.

For all CARRIBA flights a mean τ = 12.8 with a standard deviation of 4.5 was observed together with a mean r_{eff} = 10.5 µm with a standard deviation of 2.3 µm, and a mean LWC = 0.34 g m^{-3} with a standard deviation of 0.09 g m^{-3}. Differences between CARRIBA$_{\text{WET}}$ and CARRIBA$_{\text{DRY}}$ are in the range of the measurement uncertainty, with slightly lower τ and higher r_{eff} in 2011.

The small-scale inhomogeneities were covered by ground based downward radiance ($I_{\lambda}^{\downarrow}$) measurements of the hyper-spectral sensor AisaEAGLE. Figure 13a shows an almost 5 min extract of AisaEAGLE measurements (645 nm wavelength) for a typical trade wind cumulus, recorded on 20 April 2011. This sequence covered areas with clear sky (C), clouds (B), and thus also a cloud edge (A) which is significantly brighter. The Sun's position is at the center of the image. The image shows that AisaEAGLE can resolve cloud edges with a sufficient spatial resolution to study the transition between cloud and clear sky where the aerosol and particles will interact. These measurements will help to interpret the in situ observations of ACTOS in the entrainment zone of cloud edges.

Radiance spectra from the three areas (cloud, cloud edge and clear sky) $I_{\lambda}^{\downarrow}$ are plotted in Fig. 13b. All three spectra show significantly different spectral patterns. While the clear sky observations are generally dark (low radiance) and dominated by short

ACPD
12, 28609–28660, 2012

wavelengths (Rayleigh scattering) clouds are much brighter and show spectral neutrality (Mie scattering) outside of absorption bands. The radiance measured at the vicinity of the cloud edge reveals a significant enhancement of radiance which may result from a humidification and associated hygroscopic growth of the aerosol particles but is also affected by 3-D-radiative effects in adjacent cloud areas of broken clouds. The spectral data of the AisaEAGLE will allow to identify which of both effects is dominating in each case dependent on the aerosol properties measured by ACTOS (Marshak et al., 2008).

4.4 Turbulence in the Sub-Cloud and Cloud Layer

The onset of shallow cumulus convection is mainly determined by the turbulent structure, thermodynamic properties, the vertical extend of the SCL, and the structure of the interfacial layer (IL). The later connects the well-mixed SCL and the conditional unstable layer above. The high-rate measurements during CARRIBA provide an excellent opportunity to investigate the structure of these layers in more detail. Here, we focus more on the IL characterized by a slight temperature inversion and a more pronounced jump of humidity. Due to a comparable homogeneous and stationary sea surface temperature the mean height of the IL is about 500 m but the local and temporal variability is of interest.

Dolphin-like flight patterns have been performed with ACTOS during the flight on 9 April 2011 under cloud-free conditions (e.g. no clouds in the measurement area). The profiles were taken between 300 and 800 m a.s.l. (see top panel of Fig. 14 which shows the measurement height of the entire flight period). The middle panel of Fig. 14 shows the vertical profile of the specific humidity q. The first profile has the original values, all other profile are shifted by $2\,\mathrm{g\,kg^{-1}}$ to each other for better resolution. The lower panel shows the local standard deviation of the vertical wind velocity σ_w^2 as an indicator of turbulence. A high-pass filter (Savitzky-Golay filter, Savitzky and Golay, 1964) was applied to the 100 Hz data with a window of 200 samples to define the residuals. A running mean with a window of 200 samples was applied to the squared residuals to estimate the local variance.

ACPD
12, 28609–28660, 2012

For most of the profiles the height of the IL is quite obvious for q and σ_w^2. For q, the values sometimes jump or sometimes gradually decrease from typically 15 g kg^{-3} in the SCL to about 13 g kg^{-3} in the layer above. The structure of q in the SCL is always highly turbulent whereas in the stable layer variability is minor by definition. The local height of the IL covers the full range of the measurement heights. For the second profile for example the IL can be hardly detected in 350 m, for the 7th profile the top of the SCL is reached in 800 m.

Such kind of Dolphin-like flights have been performed in order to investigate the IL structure and height during four additional flights of CARRIBA$_{DRY}$ – all flights with clouds in the measurement area, although the profiling has been done out of clouds conditions only.

Another important topic in terms of cloud turbulence is the dynamic at the edge of shallow cumulus clouds. Due to its significance for mixing and entrainment cloud edge turbulence is key for understanding cloud evolution and lifetime.

In a simplified picture, cloud dynamics can be described by a strong updraft in the cloud core region which is responsible for the main growth of the cloud in the vertical direction. At cloud edge however a downward flow – mainly due to mass compensation and due to evaporative cooling with subsequent buoyancy reversal – is predominant (Heus and Jonker, 2008). These two opposite flow regimes lead to a horizontal wind shear at cloud edge, which results in further small-scale mixing.

To illustrate our measurements in terms of small-scale turbulence, a single cloud passage is shown in Fig. 15. A LWC > 0 g kg^{-3} denotes the cloud region (blue area). Inside the cloud core a peak updraft of 5 m s^{-1} is measured (green line for the vertical velocity component w), whereas at the cloud edge a downdraft of $w = -1$ m s^{-1} is observed which results in a strong horizontal wind shear between both regimes at cloud edge. Based on the high spatial resolution ($\sim$ 5 cm) of our de-spiked hot-wire measurements, we were able to estimate local energy dissipation rates $\overline{\varepsilon}_\tau$ derived from second-order structure functions (see Siebert et al., 2010, for more details of this method). The local

ACPD
12, 28609–28660, 2012

values of ε are estimated by applying a moving window with a width of 0.2 s for which $\overline{\varepsilon}_\tau$ is derived (see black line in Fig. 15)

The cloud region is characterized by intense small-scale turbulence indicated by a sharp increase of $\overline{\varepsilon}_\tau$ inside the cloud by about three orders of magnitude.

The inlay in Fig. 15 shows a 30 m wide enlarged section of the left cloud edge. It is quite obvious that the highly turbulent part already starts outside the cloud and a 3 to 5 m thick turbulent area has developed which surrounds the cloud. The influence of these turbulent shells to the entrainment process will be one major topic of further analysis.

Often it is not explicit to isolate single clouds with a distinct downdraft region at cloud edge in a cumulus field since it is hard to tell where a single cloud starts or were they do overlap with the following cloud. Nevertheless, we managed to select about 200 clouds from both campaigns for further analysis of the small-scale dynamics at cloud edges.

5 Summary

This article provides a general introduction to the two CARRIBA campaigns performed in the climatic wet season (November 2010) and dry season (April 2011) on Barbados. With the helicopter-borne ACTOS and SMART-HELIOS payloads 31 research flights have been conducted, which were supported by additional ground-based aerosol observations and remote-sensing at the East coast of Barbados. The goal of this project was to explore the fine-scale structure of trade wind cumuli with a focus on cloud microphysics, aerosol, radiation, and turbulent processes and their various interactions and feedbacks. As one unique feature of this campaign, all airborne and ground-based measurements have been realized in a comparable small square area of roughly 100 km^2 off the coast which allows an optimal inter-comparison of the different observations.

ACPD
12, 28609–28660, 2012

Even though most flights were performed under quite similar conditions in terms of the macroscopic cloud structure – fluffy shallow trade wind cumuli often combined with a few thin stratiform layers were prevailing – the microscopic structure below and in cloud, in terms of aerosol and mean cloud droplet size, was highly variable. On different flights the observed effective radii span a range between 7 and 18 µm. The two campaigns had slightly different characteristics in terms of the aerosol loading and aerosol origin. In general, during both campaigns, phases with low and high particle number concentrations occurred, with values as low as 100 cm^3 (typical clean marine conditions) and higher than 500 cm^3 (typical polluted conditions). In general, increased particle number concentrations in the CCN size range were observed often when air masses originated from Africa. During $CARRIBA_{WET}$, these aerosols were a mixture of dust and aerosol from biomass burning, while during $CARRIBA_{DRY}$ the aerosols originating from Africa were mainly dust. Additionally, during $CARRIBA_{DRY}$ measurements were made in clouds influenced by biomass burning aerosol from the Caribbean. Alltoghether, a wide range of different situations in terms of aerosol loading was observed during the two campaigns which allows us to investigate the influence of aerosol on the cloud microstructure.

In this article, after a general overview of the meteorological, aerosol, and cloud conditions the four main topics of the CARRIBA campaign were briefly introduced by presenting selected measurement examples including a discussion of their significance for the entire project.

The experiment was designed such that as many aspects as possible concerning the lifetime cycle of shallow cumulus could be covered. This starts with a detailed physical aerosol characterization including CCN measurements at ground. With similar instrumentation on ACTOS and the close collocation of the airborne and ground-based observations we are able to judge how representative the ground-based observations are for the cloud base level. With similar concentrations of total particle number concentrations on ground and in the well-mixed SCL we can safely conclude that for our

ACPD
12, 28609–28660, 2012

measurements the detailed ground-based measurements are representative also for the cloud level.

During all flights with appropriate in-situ droplet measurements substantial particle counts associated with large particles in the cloud free regions of the sub-cloud and cloud layer have been observed. The origin of these particles with typical number concentrations of ~0.5–1 cm^{-3} is not yet clear but most likely these particles are hygroscopically grown not activated sea-salt particles. The role of these particles in particular for the generation of larger cloud droplets is controversially discussed in recent literature (Colon-Robles et al., 2006; Hudson et al., 2011) and will be investigated in more detail.

An important aspect of cloud lifetime is the entrainment of sub-saturated air into the clouds with subsequent mixing and its consequences for cloud microphysical properties. Due to the fluffy appearance of the trade wind clouds, it is obvious that entrainment/detrainment and turbulent mixing play a major role in the lifetime of these clouds. Based on the high resolution of our measurements, the turbulent transition layer between cloud and environment – often observed to be only a few meters thick – can be resolved and the dynamics of the cloud edges can be described in much more detail compared with aircraft observations with less resolution.

Cloud edges with their humid environment are also known to produce highly favorable conditions for the production of new aerosol particles. This feature has been frequently observed during nearly all of our flights, with the observations being irregularly distributed in time and space. That is, the cloud has to be considered not only as an aerosol sink but also as an aerosol source. The significance of these freshly produced aerosol particles to the overall particle concentration including CCN will be investigated in more detail and discussed as one possible feedback to the onset of clouds.

Finally, the interpretation of the accompanying cloud radiation measurements benefits from a new experimental design in terms of the close collocation of the radiation and cloud measurements. In a horizontal plane the separation of the ACTOS measure-

ACPD
12, 28609–28660, 2012

ments and the radiance measurements performed by SMART-HELIOS are in the order of approximately ten meters – never obtainable with two vertically separated aircraft.

The two CARRIBA campaigns, together with data available from the MPI-M BOC, provides us with a large data-set which we will explore in more detail. This article outlined the conditions we encountered during the measurements in general, and gave a first overview of topics that will be examined more deeply in the near future.

Acknowledgements. We thank the experienced and highly engaged pilots Alwin Vollmer and Milos Kapetanovic for the terrific and safe helicopter flights in the Caribbean. Thanks also to Paul Archer from Horizon Helicopters and to National Helicopters in Canada for organizing and providing the helicopter service. Many thanks also to the team from the Barbados Concorde Experience who hosted the ACTOS and helicopter team. We thank Joe Prospero for access to his infrastructure at Ragged Point. Lutz Hirsch and Friedhelm Jansen are acknowledged for their help and experience during the preparation phase of the campaigns. We are grateful to Christoph Klaus and Dieter Schell from the enviscope company for their excellent technical support during the campaigns and acknowledge Damien Prescod from CIMH for his support in terms of local logistics. We thank Albert Ansmann for help with the interpretation of lidar data and gratefully acknowledge Deutsche Forschungsgemeinschaft (DFG) for funding this project (SI 1534/3-1 and WE 1900/18-1).

The service charges for this open access publication
have been covered by the Max Planck Society.

References

Albrecht, B. A., Bretherton, C. S., Johnson, D., Scubert, W. H., and Frisch, A. S.: The Atlantic Stratocumulus Transition Experiment – ASTEX, B. Am. Meteorol. Soc., 76, 889–904, 1995. 28611

Augstein, E., Riehl, H., Ostapoff, F., and Wagner, V.: Mass and energy transports in an undisturbed atlantic trade-wind flow, Mon. Weather Rev., 101, 101–111, 1973. 28612

ACPD

12, 28609–28660, 2012

Blyth, A. M., Lasher-Trapp, S., Cooper, W. A., Knight, C. A., and Latham, J.: The role of giant and ultragiant nuclei in the formation of early radar echoes in warm cumulus clouds, J. Atmos. Sci., 60, 2557–2572, 2003. 28613

Chiu, J. C., Marshak, A., Knyazikhin, Y., Pilewski, P., and Wiscombe, W. J.: Physical interpretation of the spectral radiative signature in the transition zone between cloud-free and cloudy regions, Atmos. Chem. Phys., 9, 1419–1430, doi:10.5194/acp-9-1419-2009, 2009. 28619

Chuang, P. Y., Saw, E. W., Small, J. D., Shaw, R. A., Sipperley, C. M., Payne, G. A., and Bachalo, W.: Airborne phase doppler interferometry for cloud microphysical measurements, Aerosol Sci. Tech., 42, 685–703, 2008. 28617

Colon-Robles, M., Rauber, R. M., and Jensen, J. B.: Influence of low-level wind speed on droplet spectra near cloud base in trade wind cumulus, Gephys. Res. Lett., 33, L20814, doi:10.1029/2006GL027487, 2006. 28637

Davidson, B.: The Barbados oceanographic and meteorological experiment, B. Am. Meteorol. Soc., 49, 928–934, 1968. 28612

Gerber, H., Arends, B. G., and Ackerman, A. S.: New microphysics sensor for aircraft use, Atmos. Res., 31, 235–252, 1994. 28617

Hanuš, J., Malenovský, Z., Homolová, L., Kaplan, V., Lukeš, P., and Cudlín, P.: Potentials of the VNIR airborne hyperspectral system AISA Eagle, in: Symposium GIS Ostrava, Ostrava, CZ, 27–30 January 2008, 2008. 28619

Haywood, J. M., Pelon, J., Formenti, P., Bharmal, N., Brooks, M., Capes, G., Chazette, P., Chou, C., Christopher, S., Coe, H., Cuesta, J., Derimian, Y., Desboeufs, K., Greed, G., Harrison, M., Heese, B., Highwood, E. J., Johnson, B., Mallet, M., Marticorena, B., Marsham, J., Milton, S., Myhre, G., Osborne, S. R., Parker, D. J., Rajot, J.-L., Schulz, M., Slingo, A., Tanré, D., and Tulet, P.: Overview of the dust and biomass-burning experiment and african monsoon multidisciplinary analysis special observing period-0, J. Geophys. Res., 113, D00C17, doi:10.1029/2008JD010077, 2008. 28613

Henrich, F., Siebert, H., Jäkel, E., Shaw, R. A., and Wendisch, M.: Collocated measurements of boundary-layer cloud microphysical and radiative properties – a feasibility study, J. Geophys. Res., 115, D24214, doi:10.1029/2010JD013930, 2010. 28619

Heus, T. and Jonker, H. J. J.: Subsiding shells around shallow cumulus clouds, J. Atmos. Sci., 65, 1003–1018, 2008. 28634

Heymsfield, A. J. and McFarquhar, G. M.: Microphysics of INDOEX clean and polluted trade cumulus clouds, J. Geophys. Res., 106, 28653–82673, 2001. 28612

ACPD
12, 28609–28660, 2012

Holland, J. Z. and Rasmusson, E. M.: Measurements of the atmospheric mass, energy, and momentum budget over a 500-kilometer square of tropical ocean, Mon. Weather Rev., 101, 44–55, 1973. 28612

Hoppel, W. A., Frick, G. M., and Larson, R. E.: Effect of nonprecipitating clouds on the aerosol size distribution in the marine boundary-layer, Geophys. Res. Lett., 13, 125–128, 1986. 28628

Hudson, J. G., Vandana, J., and Noble, S.: Drizzle correlations with giant nuclei, Geophys. Res. Lett., 38, L05808, doi:10.1029/2010GL046207, 2011. 28637

Kaufman, Y. J., Koren, I., Remer, L. A., Rosenfeld, D., and Rudich, Y.: The effect of smoke, dust, and pollution aerosol on shallow cloud development over the Atlantic Ocean, P. Natl. Acad. Sci. USA, 102, 11207–11212, 2005. 28612, 28613

Langmuir, I.: The production of rain by a chain reaction in cumulus clouds at temperature above freezing, J. Meteorol., 5, 175–192, 1948. 28612

Malkus, J. S.: Some results of a trade-cumulus cloud investigation, J. Meteorol., 11, 220–237, 1954. 28612

Malkus, J. S.: On the maintenance of the trade winds, Tellus, 8, 335–350, 1956. 28612

Malkus, J. S.: On the structure of the trade wind moist layer, Pap. Phys. Oceanogr. Meteorol., 12, 1–47, 1958. 28612

Marshak, A., Wen Jr., G., J. A. C., Remer, L. A., Loeb, N. G., and Cahalan, R. F.: A simple model for the cloud adjacency effect and the apparent bluing of aerosols near clouds, J. Geophys. Res., 113, D14S17, doi:10.1029/2007JD009196, 2008. 28619, 28633

Mayer, B.: Radiative transfer in the cloudy atmosphere, Eur. Phys. J. Conf., 1, 75–99, 2009. 28631

Mayer, B. and Kylling, A.: Technical note: The libRadtran software package for radiative transfer calculations – description and examples of use, Atmos. Chem. Phys., 5, 1855–1877, doi:10.5194/acp-5-1855-2005, 2005. 28631

Perry, K. D. and Hobbs, P. V.: Further evidence for particle nucleation in clear air adjacent to marine cumulus clouds., J. Geophys. Res., 99, 22803–22818, 1994. 28630

Petters, M. D. and Kreidenweis, S. M.: A single parameter representation of hygroscopic growth and cloud condensation nucleus activity, Atmos. Chem. Phys., 7, 1961–1971, doi:10.5194/acp-7-1961-2007, 2007. 28629

ACPD

12, 28609–28660, 2012

Pringle, K. J., Tost, H., Pozzer, A., Pöschl, U., and Lelieveld, J.: Global distribution of the effective aerosol hygroscopicity parameter for CCN activation, Atmos. Chem. Phys., 10, 5241–5255, doi:10.5194/acp-10-5241-2010, 2010. 28629

Prospero, J. M. and Carlson, T. N.: Vertical and areal distribution of Saharan dust over the Western Equatorial North Atlantic Ocean, J. Geophys. Res., 77, 5255–5265, 1972. 28613

Prospero, J. M. and Lamb, P. J.: African droughts and dust transport to the Caribbean: climate change implications, Science, 302, 1024–1027, 2003. 28620

Rauber, R. M., Stevens, B., Ochs, H. T., Knight, C., Albrecht, B. A., Blyth, A. M., Fairall, C. W., Jensen, J. B., Lasher-Trapp, S. G., Mayol-Bracero, O. L., Vali, G., Anderson, J. R., Baker, B. A., Bandy, A. R., Burnet, F., Brenguier, J.-L., Brewer, W. A., Brown, P. R. A., Chuang, P., Cotton, W. R., Di Girolamo, L., Geerts, B., Gerber, H., Göke, S., Gomes, L., Heikes, B. G., Hudson, J. G., Kollias, P., Lawson, R. P., Krueger, S. K., Lenschow, D. H., Nuijens, L., O'Sullivan, D. W., Rilling, R. A., Rogers, D. C., Siebesma, A. P., Snodgrass, E., Stith, J. L., Thornton, D. C., Tucker, S., Twohy, C. H., and Zuidema, P.: Rain in shallow cumulus over the ocean, B. Am. Meteorol. Soc., 88, 1912–1928, 2007. 28612

Reid, J. S., Westphal, D. L., Livingston, J. M., Savoie, D. L., Maring, H. B., Jonsson, H. H., Eleuterio, D. P., Kinney, J. E., and Reid, E. A.: Dust vertical distribution in the Caribbean during the Puerto Rico Dust Experiment, Geophys. Res. Lett., 29, 1151, doi:10.1029/2001GL014092, 2002. 28613

Roberts, G. and Nenes, A.: Miniaturizing the continous-flow streamwise thermal-gradient CCN chamber, in: Proceedings of the 7th International Aerosol Conference, vol. 1, St. Paul, USA, 448–449, 2006. 28620

Roberts, G. C. and Nenes, A.: A continuous-flow streamwise thermal-gradient CCN chamber for atmospheric measurements, Aerosol Sci. Tech., 39, 206–221, 2005. 28618, 28620

Rudich, Y., Khersonsky, O., and Rosenfeld, D.: Treating clouds with a grain of salt, Geophys. Res. Lett., 29, 2060, doi:10.1029/2002GL016055, 2002. 28613

Savitzky, A. and Golay, M.: Smoothing and differentiation of data by simplified least squares procedures, Anal. Chem., 36, 1627–1639, 1964. 28633

Schmidt, K. S., Feingold, G., Pilewskie, P., Jiang, H., Coddington, O., and Wendisch, M.: Irradiance in polluted cumulus fields: measured and modeled cloud-aerosol effects, Geophys. Res. Lett., 36, L07804, doi:10.1029/2008GL036848, 2009. 28619

ACPD
12, 28609–28660, 2012

Siebert, H., Franke, H., Lehmann, K., Maser, R., Saw, E. W., Schell, D., Shaw, R. A., and Wendisch, M.: Probing fine-scale dynamics and microphysics of clouds with helicopter-borne measurements, B. Am. Meteorol. Soc., 87, 1727–1738, 2006. 28617

Siebert, H., Shaw, R. A., and Warhaft, Z.: Statistics of small-scale velocity fluctuations and internal intermittency in marine stratocumulus clouds, J. Atmos. Sci., 67, 262–273, 2010. 28634

Smirnov, A., Holben, B. N., Savoie, D., Prospero, J. M., Kaufman, Y. J., Tanre, D., Eck, T. F., and Slutsker, I.: Relationship between column aerosol optical thickness and in situ ground based dust concentrations over Barbados, Geophys. Res. Lett., 27, 1643–1646, 2000. 28613

Stevens, B.: On the growth of layers of non-precipitating cumulus convection, J. Atmos. Sci., 64, 2916–2931, 2007. 28612

Stevens, B. and Feingold, G.: Untangling aerosol effects on clouds and precipitation in a buffered system, Nature, 461, 607–613, 2009. 28613

Stommel, H.: Entrainment of air into a cumulus cloud, J. Meteorol., 4, 91–94, 1947. 28612

Stommel, H.: Entrainment of air into a cumulus cloud II, J. Meteorol., 8, 127–129, 1951. 28612

Tiedtke, M.: A comprehensive mass flux scheme for cumulus parameterization in large-scale models, Mon. Weather Rev., 117, 1779–1800, 1989. 28611

Twomey, S.: The influence of pollution on the shortwave albedo of clouds, J. Atmos. Sci., 34, 1149–1152, 1977. 28613

Wehner, B., Siebert, H., Ansmann, A., Ditas, F., Seifert, P., Stratmann, F., Wiedensohler, A., Apituley, A., Shaw, R. A., Manninen, H. E., and Kulmala, M.: Observations of turbulence-induced new particle formation in the residual layer, Atmos. Chem. Phys., 10, 4319–4330, doi:10.5194/acp-10-4319-2010, 2010. 28618

Wehner, B., Siebert, H., Hermann, M., Ditas, F., and Wiedensohler, A.: Characterisation of a new Fast CPC and its application for atmospheric particle measurements, Atmos. Meas. Tech., 4, 823–833, doi:10.5194/amt-4-823-2011, 2011. 28618

Wendisch, M. and Brenguier, J.-L., Eds.: Airborne Measurements for Environmental Research: Methods and Instruments, Wiley-VCH Verlag GmbH & Co. KGaA, Weinheim, Germany, ISBN: 978-3-527-40996-9, 2013. 28617

Werner, F., Siebert, H., Pilewskie, P., and Wendisch, M.: Helicopter-borne passive remote sensing and collocated in situ observations of microphysical and optical properties of trade wind cumuli under overlying cirrus, J. Geophys. Res., in review, 2012. 28619

ACPD
12, 28609–28660, 2012

Woodcock, A. H., Kientzler, C. F., Arons, A. B., and Blanchard, D. C.: Giant condensation nuclei from bursting bubbles, Nature, 172, 1144–1145, 1953. 28613
Yuskiewicz, B. A., Stratmann, F., Birmili, W., Wiedensohler, A., Swietlicki, E., Berg, O., and Zhou, J.: The effects of in-cloud mass production on atmospheric light scatter, Atmos. Res., 50, 256–288, 1999. 28629

ACPD
12, 28609–28660, 2012

Table 1. Schedule of all research flights during CARRIBA$_{WET}$ in 2010 and CARRIBA$_{DRY}$ in 2011.

	Flight No	Date	DOY	Start UTC	Landing UTC	Duration min
	#01	2010-11-12	316	14:17	15:38	1:21
C	#02	2010-11-12	316	18:51	20:27	1:35
A	#03	2010-11-13	317	13:14	14:37	1:22
R	#04	2010-11-13	317	17:45	19:23	1:38
R	#05	2010-11-14	318	17:26	18:55	1:28
I	#06	2010-11-15	319	14:07	15:40	1:32
B	#07	2010-11-16	320	14:43	15:54	1:10
A	#08	2010-11-20	324	16:52	18:40	1:48
	#09	2010-11-21	325	13:30	15:21	1:50
D	#10	2010-11-21	325	18:45	20:46	2:01
R	#11	2010-11-22	326	13:53	15:44	1:50
Y	#12	2010-11-23	327	13:32	15:34	2:01
	#13	2010-11-24	328	13:29	15:25	1:56
	#14	2010-11-25	329	13:31	15:24	1:52
	#15	2010-11-26	330	14:00	15:47	1:47
	#16	2010-11-27	331	13:31	15:26	1:54

ACPD
12, 28609–28660, 2012

Table 1. Continued.

	Flight No	Date	DOY	Start UTC	Landing UTC	Duration min
	#17	2011-04-09	99	13:30	15:08	1:36
C	#18	2011-04-10	100	13:44	15:29	1:44
A	#19	2011-04-13	103	13:47	15:28	1:40
R	#20	2011-04-14	104	13:53	15:46	1:53
R	#21	2011-04-14	104	19:35	21:35	1:59
I	#22	2011-04-15	105	13:41	15:24	1:43
B	#23	2011-04-16	106	13:39	15:23	1:44
A	#24	2011-04-18	108	13:44	15:29	1:44
	#25	2011-04-19	109	13:04	14:47	1:42
W	#26	2011-04-19	109	18:30	20:23	1:52
E	#27	2011-04-20	110	14:27	16:21	1:53
T	#28	2011-04-22	112	13:29	15:22	1:53
	#29	2011-04-23	113	13:27	15:24	1:56
	#30	2011-04-24	114	14:13	16:07	1:54
	#31	2011-04-25	115	13:50	15:42	1:51

ACPD
12, 28609–28660, 2012

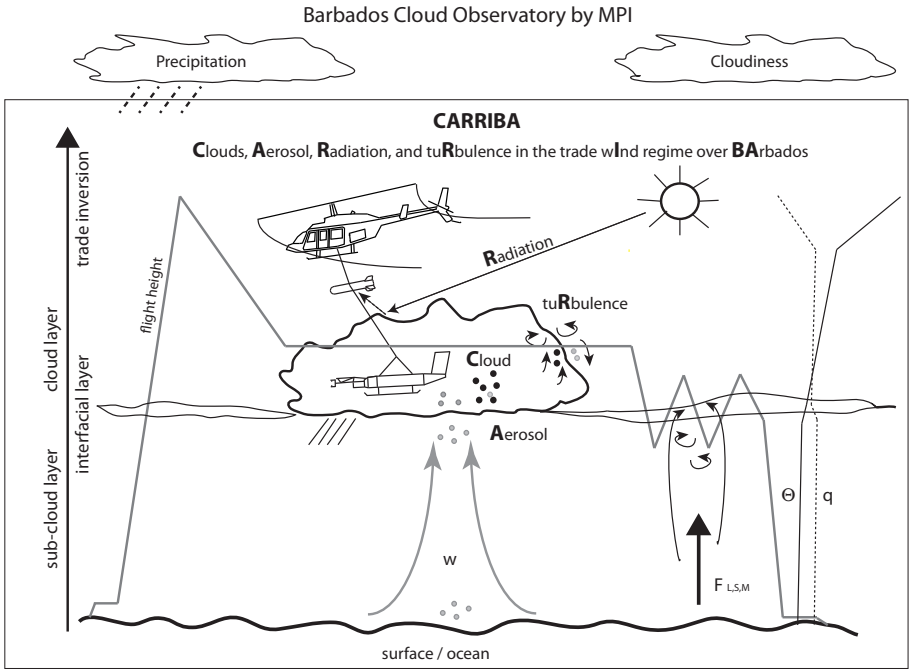

Fig. 1. The cartoon illustrates the cloud processes of the four main topics of the CARRIBA project: Clouds, Aerosol, Radiation, and tuRbulence in trade wInd regime over BArbados and how the helicopter-borne measurements are embedded in the long-term remote-sensing observations in terms of cloudiness and precipitation performed at the Barbados Cloud Observatory (BCO).

ACPD
12, 28609–28660, 2012

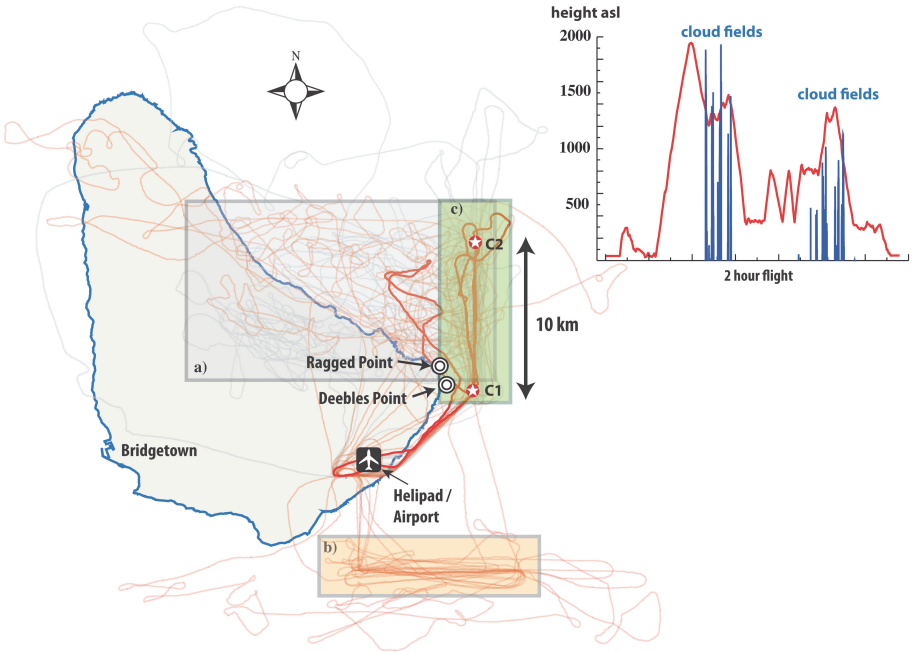

Fig. 2. A map of Barbados including the location of the helipad for the ACTOS operation and the two stations at Deebles Point and Ragged Point. For both campaigns the tracks of all ACTOS flights are shown, the orange lines are for $CARRIBA_{WET}$ and the gray lines are for $CARRIBA_{DRY}$, respectively. The three main operational areas are marked by colored boxes: (a) area were about 80 % of the cloud sampling took place, (b) alternative area only used during the first flights of $CARRIBA_{WET}$ for conditions with higher commercial traffic load, and (c) box with the two navigation points C1 and C2 for profiling. The flight of 19 April 2011 is marked as red line. For this example the measurement height is presented in the upper right panel together with sampled clouds (blue lines) to illustrate the flight strategy.

ACPD
12, 28609–28660, 2012

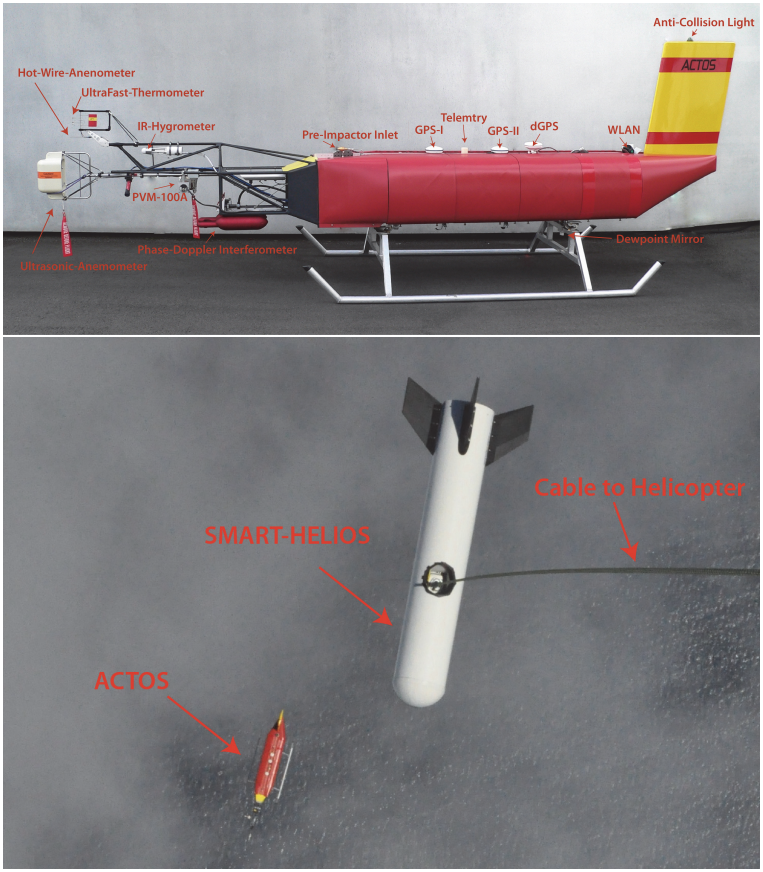

Fig. 3. Upper panel: ACTOS with its main sensors located at the carbon fibre outrigger. The data acquisition, sensors electronics, and power supply are located in the 19″-racks behind the red covers. Lower panel: ACTOS with SMART-HELIOS entering a field of fluffy cumulus clouds over the Caribbean Ocean.

ACPD
12, 28609–28660, 2012

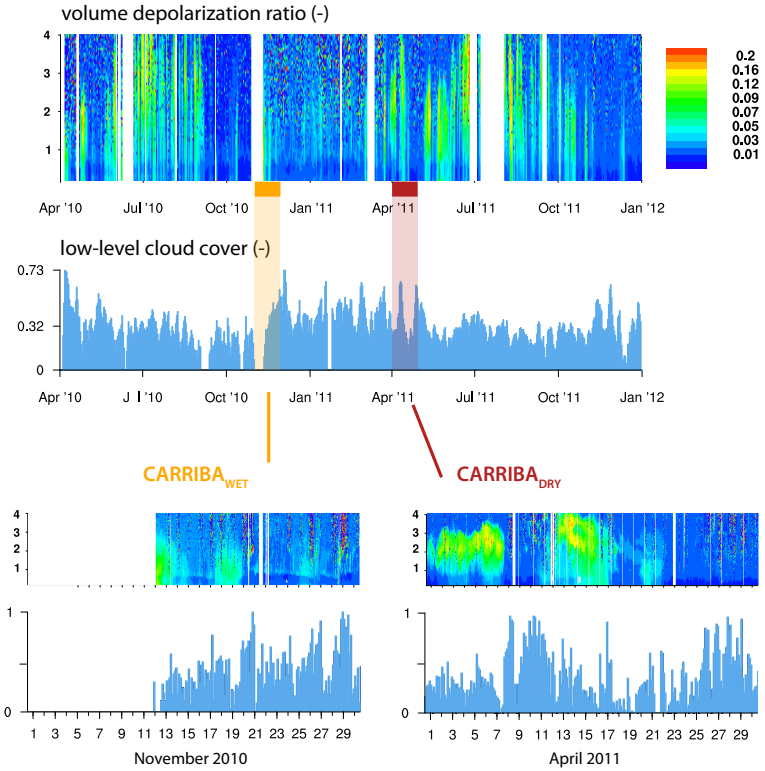

Fig. 4. Time series of volume depolarization ratio measured by the Raman lidar and ceilometer-derived low level cloud cover (fraction of time with a cloud base height < 5 km) both measured at BCO. Below are zoom-ins on the two CARRIBA periods in November 2010 and April 2011. The long data gap at the beginning of $CARRIBA_{WET}$ was due to a power outage related to the hurricane Tomas that passed over Barbados.

ACPD
12, 28609–28660, 2012

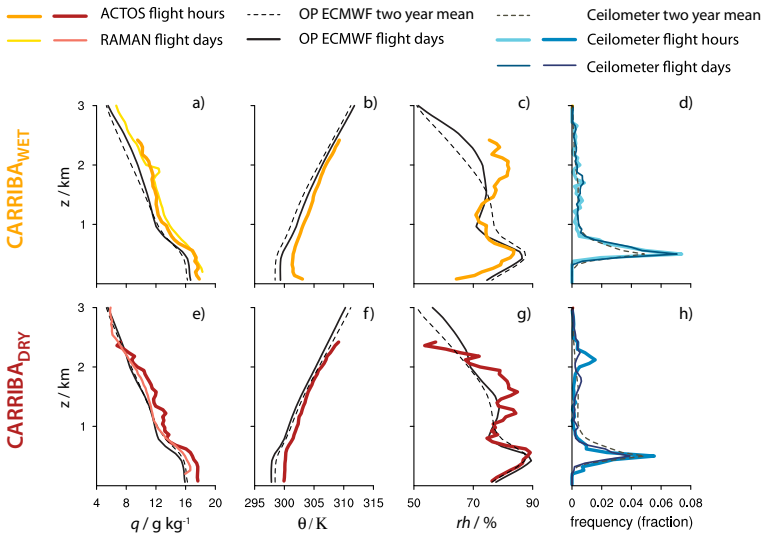

Fig. 5. Profiles of specific humidity q (**a** and **e**), potential temperature θ (**b**, **f**), relative humidity rh (**c**, **g**), and the vertical distribution of cloud base heights (**d**, **h**). Black dashed lines show the two year mean humidity and temperature profiles, derived from ECMWF operational analysis (12:00 UTC) for a single grid-point near Barbados, and two year of ceilometer-derived cloud base heights. The mean profiles during ACTOS flight days only are shown as black solid lines (EMCWF OP) and dark blue solid lines (ceilometer). The RAMAN lidar humidity profiles during 07:00–09:00 UTC on ACTOS flight days are shown as yellow and pink. Profiles measured by ACTOS are shown as thick orange and red lines, and the corresponding cloud base heights as thick light and dark blue lines. Top panels are for $\text{CARRIBA}_{\text{WET}}$, bottom panels are the same, but for $\text{CARRIBA}_{\text{DRY}}$.

ACPD
12, 28609–28660, 2012

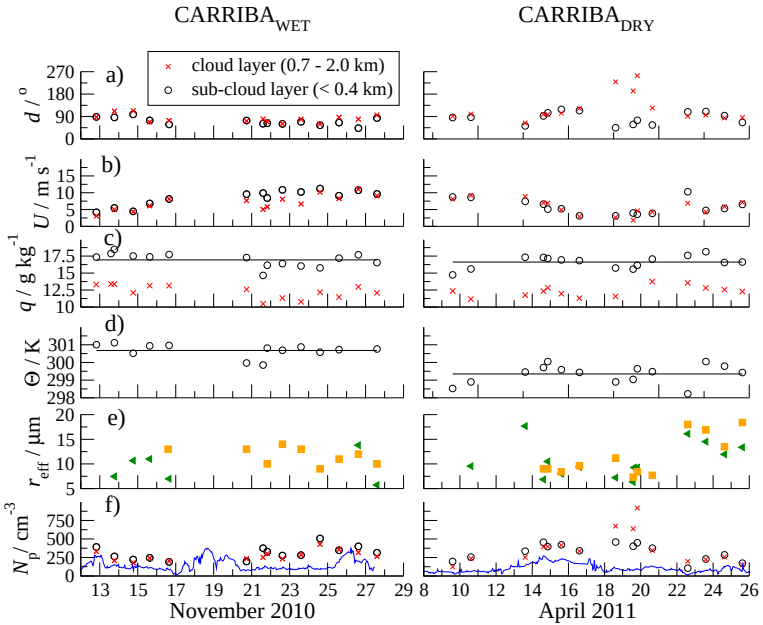

Fig. 6. Overview of the meteorological situation during CARRIBA$_{WET}$ and CARRIBA$_{DRY}$. Displayed are mean values representative for the SCL below 400 m (black circles) and the cloud-free layer in the height range between 0.7 and 2.0 km (red crosses). Only data from over the ocean is considered for the SCL height. Displayed are the mean wind direction d, the mean horizontal wind velocity U, the specific humidity q, the potential temperature Θ, and the aerosol particle number concentration N_p. The solid blue line represents the particle number concentration with diameters > 80 nm (a proxy for CCN at $S \approx 0.2$ %) as continuously measured at Ragged Point. The mean effective radius r_{eff} is estimated for cloud fields in the height range between 0.7 and 2.0 km, the orange symbols are in-situ estimates derived from the PDI and the green symbols are retrievals from radiation measurements representative for cloud top.

ACPD
12, 28609–28660, 2012

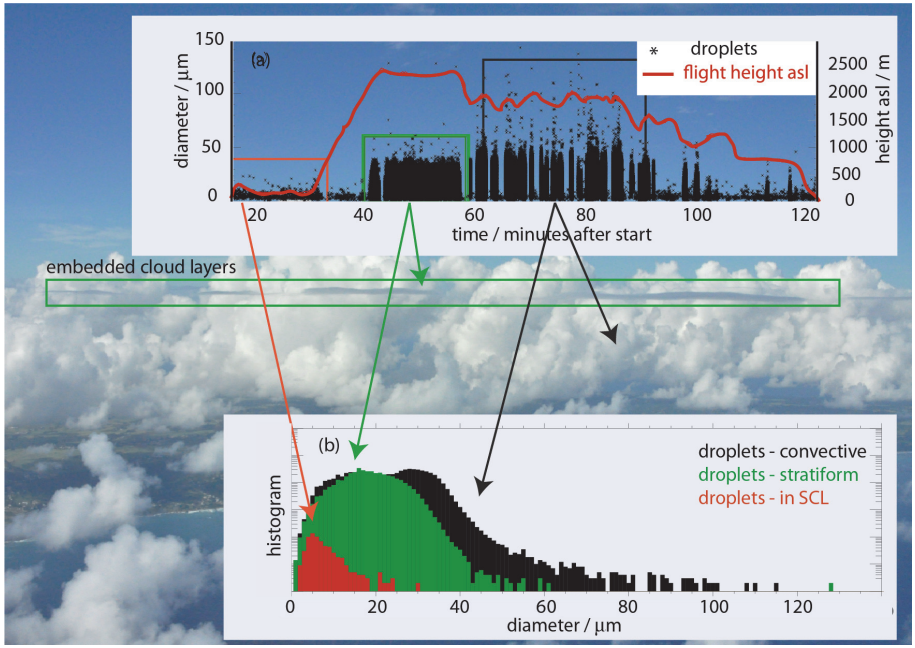

Fig. 7. Droplet measurements during a typical cloud situation (#13) with shallow cumulus and thin embedded cloud layers (marked with green box in the picture). The upper panel shows the time series of droplet diameter (each black symbol marks one single droplet). The red line indicates the flight height a.s.l. Three different regions are marked with boxes: (i) particles measured in the SCL (red box), (ii) embedded stratiform layers (green box), and (iii) shallow cumulus clouds (black box). The three histograms for the three types are shown in the lower panel with the color code.

ACPD
12, 28609–28660, 2012

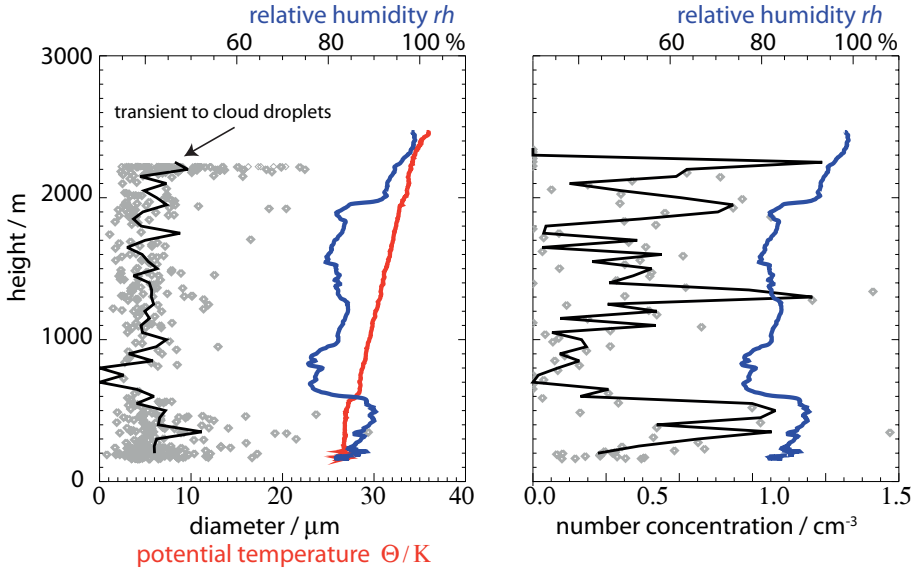

Fig. 8. Left panel shows vertical profile of particle diameter, potential temperature Θ (shifted by 273 K) and rh and the right panel shows vertical profile of particle number concentration (10 s mean) and rh. All profiles are sampled during the first ascent (cf. Fig. 7).

ACPD
12, 28609–28660, 2012

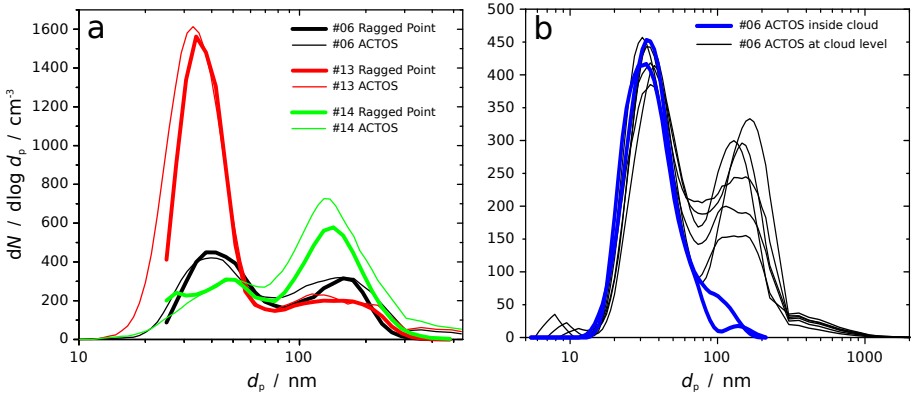

Fig. 9. Aerosol particle number size distributions. **(a)** shows a comparison of a size distribution measured on ACTOS in the SCL (thin lines) and simultaneously at Ragged Point (thick lines) during three different research flights (#06, #13 & #14). **(b)** illustrates measurements at cloud level during #06 (black and blue lines). Thick blue lines indicate measurements of interstitial aerosol inside one cloud passage.

ACPD
12, 28609–28660, 2012

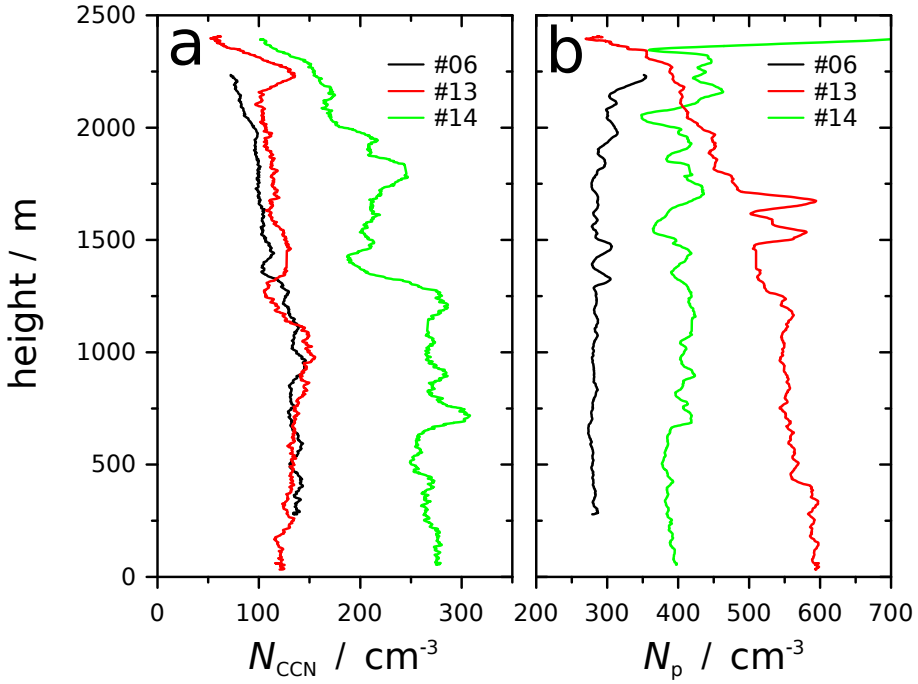

Fig. 10. Vertical profiles of CCN concentrations at 0.25 % super-saturation measured on ACTOS during three (#06, #13 & #14) different research flights **(a)**. The lines represent running averages with an averaging time of 30 s. On **(b)** vertical profiles of total particle number concentration (N_p) is plotted for the same research flights, the lines represent a 10 s running average.

ACPD
12, 28609–28660, 2012

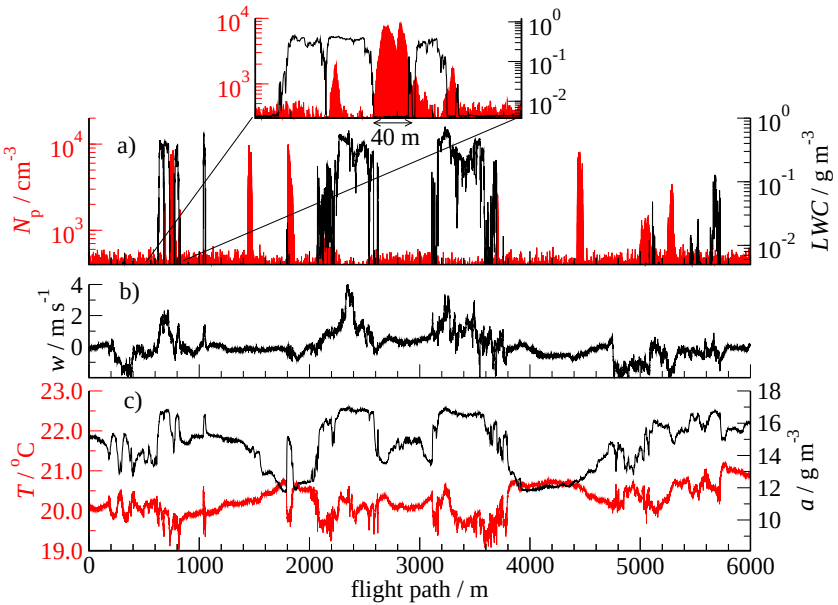

Fig. 11. In-situ observations performed with ACTOS during a 6km-long flight path in around 900 m height with several cumulus penetrations (#13). **(a)** shows the particle number concentration N_p (red line) in the size range between 6 nm and 2 µm together with the LWC (black line) as cloud indicator; for both parameters the abscissa is on a logarithmic scale. The mean background concentration is about 400 cm^{-3} with distinct peaks up to 10^4 cm^{-3}. **(b)** shows the vertical wind velocity w, whereas **(c)** indicates static temperature T (red line) and absolute humidity a (black line).

ACPD
12, 28609–28660, 2012

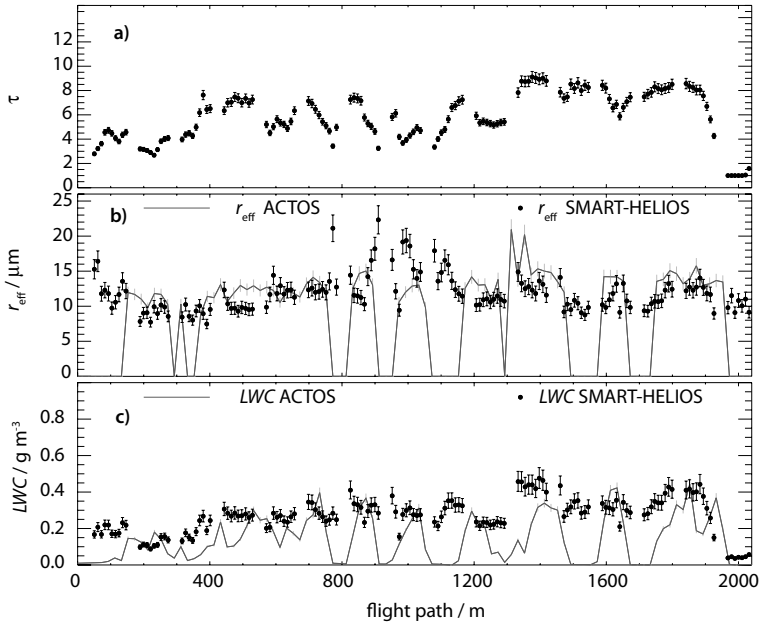

Fig. 12. (a) Cloud optical thickness τ from the SMART-HELIOS payload as a function of relative flight path. **(b)** In-situ measured r_{eff} from ACTOS and retrieved r_{eff} from SMART-HELIOS. **(c)** In-situ measured LWC from ACTOS and retrieved LWC from SMART-HELIOS.

ACPD
12, 28609–28660, 2012

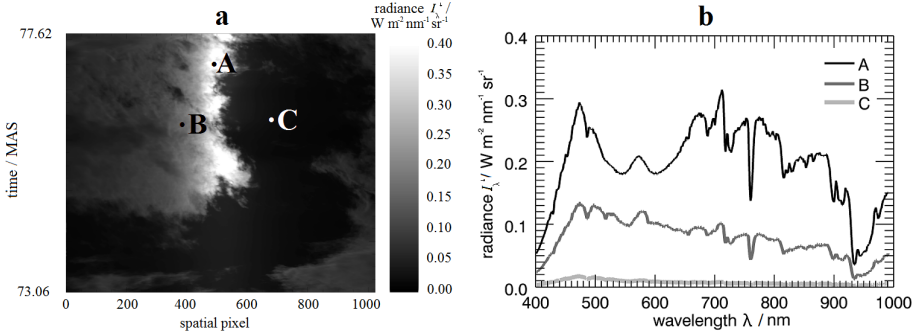

Fig. 13. (a) 5 min extract of AisaEAGLE downward radiance $I_\lambda^\downarrow$ measurements at 645 nm wavelength, recorded on 20 April 2011. **(b)** Spectral $I_\lambda^\downarrow$ for three representative areas: cloud (B), cloud edge (A) and clear sky (C).

ACPD
12, 28609–28660, 2012

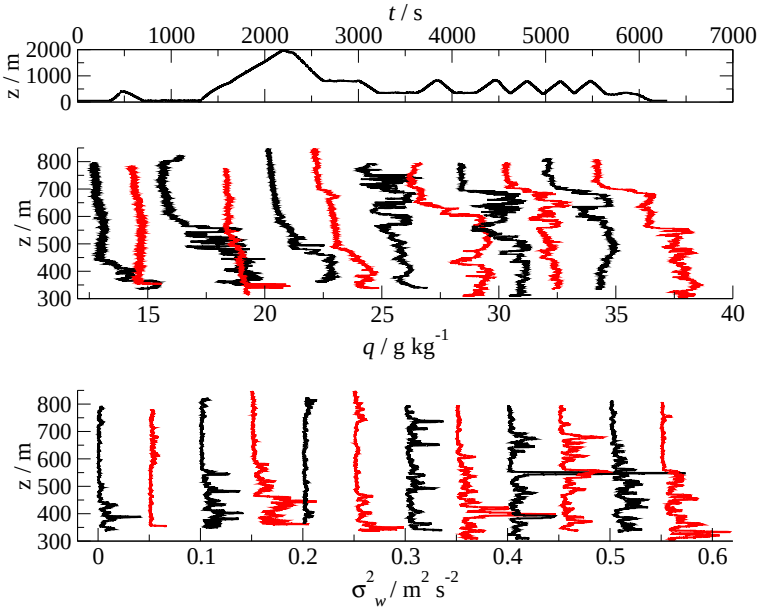

Fig. 14. Upper panel: Measurement height a.s.l. of an ACTOS flight during cloud-free conditions (#17). Dolphin-like patterns comprising twelve profiles in the height range between 300 and 800 m were flown to investigate the small-scale structure of the SCL and the IL. The middle panel shows the specific humidity q, the first profile has the original values, all other profile are shifted by $2\,\mathrm{g\,kg^{-1}}$ to each other for better resolution. In addition, red and black lines are used for a better distinguishability of subsequent profiles. The lower panel shows local variances σ_w^2 of the vertical wind velocity w.

ACPD
12, 28609–28660, 2012

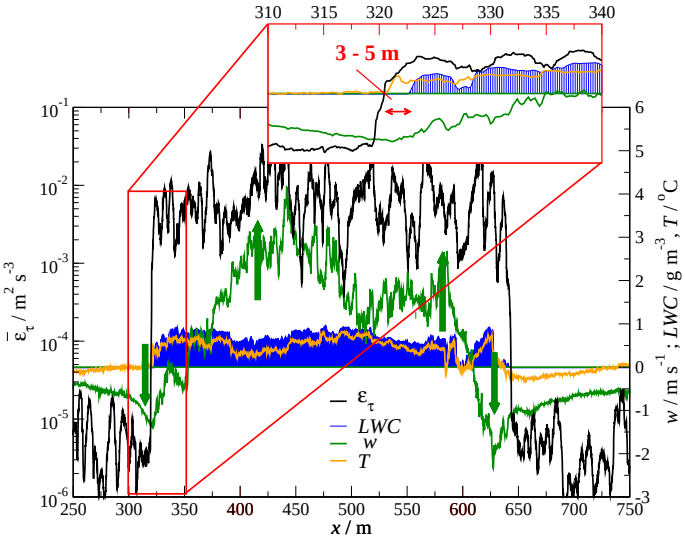

Fig. 15. A single cloud passage of a horizontal flight of 14 April 2011(#14): (a) liquid water content (LWC, blue area), (b) vertical wind velocity (w, green line), and (c) temperature (T, orange line). For the temperature the value before entering the cloud has been subtracted. In addition the local energy dissipation rate ε_τ as derived from de-spiked hot-wire data is plotted (black line). The cloud has a diameter of about 300 m. The upper inlay shows an enlarged picture of the left cloud edge where a 3 to 5 m thin highly turbulent but drop-free area at the cloud edge has been observed.

ACPD
12, 28609–28660, 2012